Glass Struct. Eng. (2018) 3:167–181
https://doi.org/10.1007/s40940-018-0062-0

SI: CHALLENGING GLASS PAPER

Experimental investigation into the fragment size of tempered glass

N. Pourmoghaddam · **J. Schneider**

Received: 13 January 2018 / Accepted: 17 March 2018 / Published online: 13 April 2018
© Springer International Publishing AG, part of Springer Nature 2018

Abstract This work presents the relation between the fragment density and the permanent residual stress in fragmented tempered glasses of various thicknesses. Therefore, fracture tests were carried out on tempered glass plates and the fragments in observation fields of 50 mm × 50 mm were counted. The average fragment density in the observation fields was set in correlation with the average measured residual stress of each specimen. Furthermore, the average particle weight of 130 particles per specimen chosen by random was determined. The relation between the average particle weight and the measured residual stress is given. The volume and the base surface as well as the radius of the particles are calculated assuming cylindrical fragments with approximately unchanged thicknesses. The relation between the residual stress and the particle base surface of regular polygonal shapes $n = 3$–8 edges in addition to the cylindrical fragment ($n \to \infty$) is also determined. The glass used for the fracture tests was commercial soda-lime-silica glass with three different thicknesses 4, 8 and 12 mm. The results in this work are a basis for the establishment of a theoretical model to predict macro-scale fracture patterns from elastic strain energy in tempered glass.

N. Pourmoghaddam (✉) · J. Schneider
Technical University of Darmstadt, Franziska-Braun-Str. 3, 64287 Darmstadt, Germany
e-mail: pourmoghaddam@ismd.tu-darmstadt.de

Keywords Fragmentation · Particle count · Particle weight · Residual stress · Tempered glass · Elastic strain energy · Heat transfer coefficient

1 Introduction

The fragmentation of tempered glass sets standards for the quality of the tempering process and the degree of safety. The European Standard EN 12150-1 defines the minimum number of fragments required for soda-lime-silica safety glass on the basis of fragmentation test results. As an example, for glass thicknesses of 4–12 mm the counted number of fragments in an observation field of 50 mm × 50 mm should not be less than 40 pcs. Several studies on the fragmentation behavior in tempered glasses showing the relation between the residual stress, glass thickness and fragment density have been reported (Acloque 1956; Akeyoshi and Kanai 1965; Barsom 1968; Gulati 1997; Shutov et al. 1998; Mognato et al. 2017). The interrelation between the glass thickness and the fragmentation behavior in tempered thin glasses with glass thicknesses 2.1–3.2 mm have been studied by Lee et al. (2012). It is known that the number of fragments is significantly dependent on the degree of tempering of the glass, i.e., to the tensile stress in the middle layer of the tempered glass. However, the main objective of this paper is to present experimental data of the fragmentation behavior in order to determine the degree of tempering required to ensure the safe character of glass fragmen-

Fig. 1 Fragmentation of tempered glass. Left: low residual stress state. Right: high residual stress state

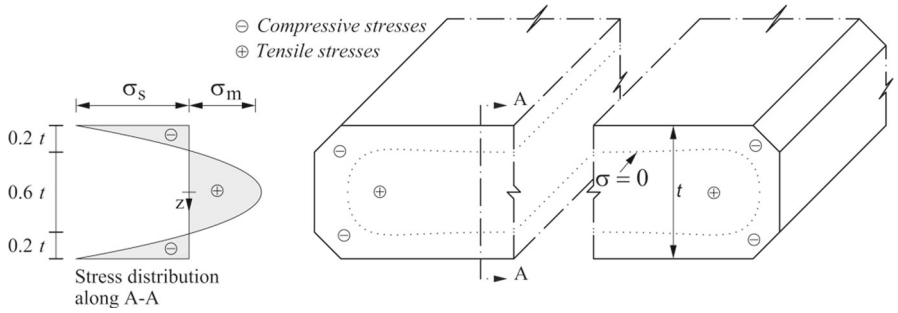

Fig. 2 Parabolic residual stress distribution along the thickness t of a tempered glass plate and the sketch of the zero stress contour line, each of the compression layers (⊖) are approx. 20% of the thickness, the tensile layer (⊕) is approx. 60% of the thickness

tation, the fragment density resulting from fracture and the average fragment size. Thermally tempered glasses will fragmentize completely, if the residual stress state within the glass plate is disturbed sufficiently (Fig. 1). The residual stress state is obtained by the thermal tempering of a glass plate and is approximately parabolic through the thickness with the compressive stress on both surfaces and an internal tensile stress in the mid-plane (Fig. 2). By imposing a compressive residual stress at the surface, the surface flaws will be in a permanent state of compression which has to be exceeded by external loading before failure can occur (Schneider 2001; Nielsen et al. 2009; Pourmoghaddam et al. 2016; Pourmoghaddam and Schneider 2018). The fragmentation is the direct consequence of the elastic strain energy that is stored inside the material due to the residual stress state. Hence, the fragment size depends on the amount of the energy released.

Considering only the stress state far away from the edges, it is reasonable to assume a homogenous planar hydrostatic stress state σ (equal in the plate plane, zero perpendicular to the plate plane and without any shear stresses) and a parabolic distribution along the thickness t of the plate. Figure 2 is showing the parabolic residual stress distribution over the thickness far from an edge. The parabolic stress distribution $\sigma(z)$ can be written in terms of the mid-plane stress σ_m as:

$$\sigma(z) = \sigma_m \left(1 - 3\zeta^2\right), \quad \zeta = \frac{2z}{t} \tag{1}$$

using the symbols which are defined in Fig. 2. Because of the parabolic distribution it can be assumed that the surface compressive stress is twice the mid-plane tensile stress in magnitude, $2\sigma_m = -\sigma_s$, and that the zero stress contour is located at a depth of approximately 20% of the thickness. Due to the parabolic stress state an elastic strain energy is established inside of the tempered glass plate, which is governing the fragmentation behavior and the subsequent fragment size (Barsom 1968; Gulati 1997; Shutov et al. 1998; Warren 2001; Tandon and Glass 2005; Nielsen 2016). Applying Hooke's law and with an assumption of the linear elastic material behavior and a homogenous planar hydrostatic stress state, as mentioned before, with the only non-zero stresses $\sigma = \sigma_x = \sigma_y \neq 0$ the elastic strain energy U can be written as:

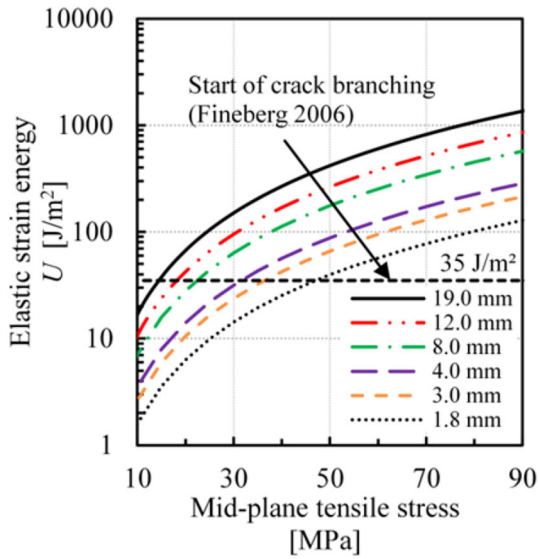

Fig. 3 Elastic strain energy U [J/m^2] versus mid-plane tensile stress [MPa], the start of crack branching according to Fineberg (2006) is marked

$$U = \frac{1-\nu}{E} \int_V \sigma(z)^2 \, dV \tag{2}$$

Inserting the residual stress distribution $\sigma(z)$ from Eq. (1) in Eq. (2) and integrating over a cube's volume with $dV = dx\,dy\,dz$, we obtain per unit area:

$$U = \frac{4}{5} \frac{(1-\nu)}{E} t \sigma_m^2 \tag{3}$$

In Fig. 3, the relation between the elastic strain energy and the residual tensile stress in the mid-plane of a glass plate dependent on its thickness is shown. The strain energy due to the residual stress increases proportional to the thickness of the glass plate. Since the fragmentation is governed by the residual stress respectively the released strain energy, for two glass plates with the same residual stress state the one with the higher thickness will fragmentize in smaller fragments than the thinner glass plate. Based on the experimental investigations in the field of dynamic fracture in brittle materials Fineberg (2006) showed, that a propagating crack branches by an energy of 35 J/m^2. We will come back to it later in this work and compare the start of crack branching by our fracture tests.

In order to study the correlation between the residual stress, particle count, particle weight and particle size, glass plates with three different thicknesses of 4, 8 and 12 mm were tempered with heat treatment conditions for a predetermined residual stress range. In Fig. 4, four examples of fracture patterns showing the fragment size for different heat treated tempered glass plates with the same thickness are shown. For the different heat treatment of the specimens the engine power of the tempering oven was estimated and varied by recalculating the air velocity and the air pressure from the iteratively determined heat transfer coefficients needed for yielding the target residual stress. After the tempering process, the residual stress in the glass specimens were measured, using a scattered light polariscope (SCALP). The glass specimens were then fractured according to EN 12150-1 and the fracture patterns were scanned using the CulletScanner desk of the company Softsolution GmbH (CulletScanner 2017). Subsequently the particles were counted and weighed. The focus of this work is on the investigation of the fragment density. Correlations between the residual stress, the fragment density and the particle weight respectively the particle volume were established. The interrelation between the residual stress and the edge length of regular polygonal shapes in addition to the cylindrical fragment is also determined.

2 Heat treatment of specimens with different heat transfer coefficients

2.1 Specimen preparation for the thermal tempering

For the fracture tests we produced three series of tempered glass specimens of size 360 mm × 1100 mm with three different thicknesses of 4, 8 and 12 mm (see Table 1). There were 24 specimens in each series divided into eight groups of three specimens for each run of the tempering process. Hence, there were eight runs of the tempering process per series for achieving the goal of eight different residual stresses in each series. In order to choose the target residual stresses for the heat treatment of the series, the elastic strain energy level for the start of the crack branching of glass according to Fineberg (2006) was considered. However, this level of energy represents the start of local crack branching by one rapidly moving tensile crack (Fineberg 2006). The question was how this level would influence the fracture pattern of a tempered glass. Therefore, in the first step the target residual stresses were chosen above as well as below the strain energy level of 35 J/m^2. As it is shown in Fig. 5, eight

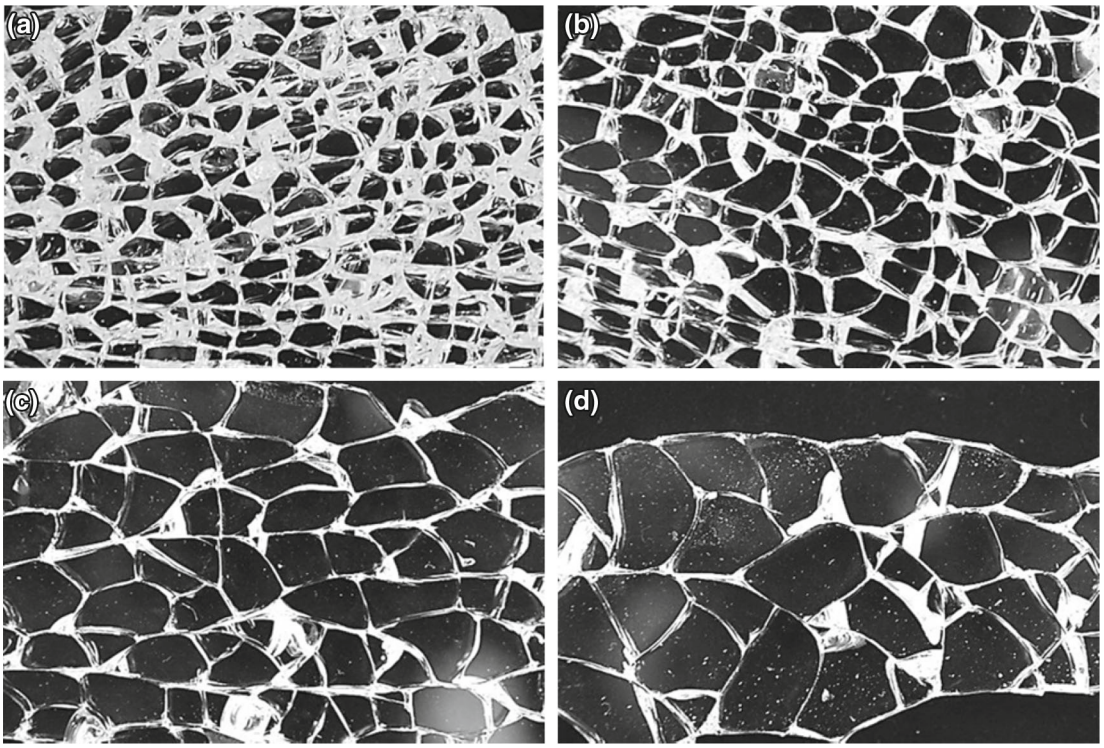

Fig. 4 Fragmentation in relation to the residual stress state (thickness $t = 12$ mm), **a** $\sigma_m = 57.9$ MPa; ($U = 354.7$ J/m^2), **b** $\sigma_m = 38.4$ MPa; ($U = 156.2$ J/m^2), **c** $\sigma_m = 31.4$ MPa; ($U = 104.1$ J/m^2), d) $\sigma_m = 27.2$ MPa; ($U = 78.1$ J/m^2)

Table 1 Series for the tempering process

Series	Specimens per series	Runs per series	Dimension [mm]	Thickness [mm]
ScA	24	8	360 × 1100	4
ScB	24	8	360 × 1100	8
ScC	24	8	360 × 1100	12

target residual mid-plane tensile stresses were chosen from 10 to 60 MPa for the 8 and 12 mm thick specimens and from 10 to 45 MPa for the 4 mm thick specimens.

For the heat treatment of the series, the engine power of the thermal tempering oven was varied. Thus, the engine power needed for the corresponding residual stress was determined considering the procedure sketched in Fig. 6. The engine power for the cooling section of the thermal tempering oven was recalculated by the determination of the required heat transfer coefficient h, which in turn leads to a certain cooling air velocity w and subsequently a required air pressure P. The engine power was then calculated considering the

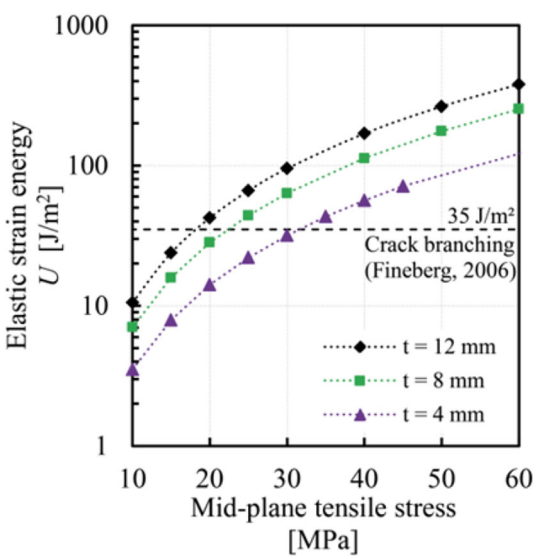

Fig. 5 Eight target mid-plane tensile stresses for the heat treatment of the series with three different thicknesses 4, 8 and 12 mm considering the level of strain energy for the start of the crack branching according to Fineberg (2006)

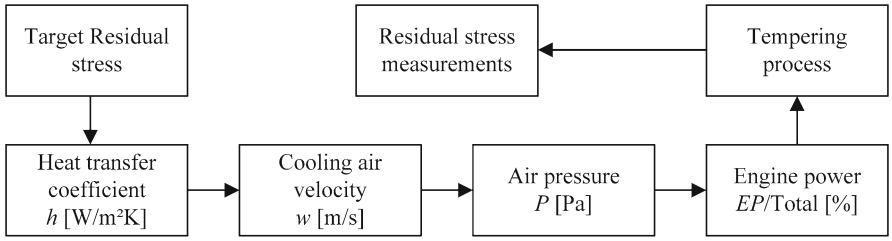

Fig. 6 Sketch of the procedure for the determination of the engine power

experience values for the relation between the adjusted engine power and the resulting air pressure P.

2.1.1 Heat transfer coefficient

The heat transfer coefficient, which is required for yielding the target residual stresses (Fig. 5), was calculated by means of a Finite Element simulation of the tempering process using an infinite 2D-axisymetric model. A FE-Model for the simulation of the thermal tempering process and the numerically calculation of the residual stresses has been discussed in detail by several authors, see e.g. Nielsen (2009), Nielsen et al. (2010), Aronen (2012), Aronen and Karvinen (2017), Pourmoghaddam and Schneider (2018). The viscoelastic material behaviour of glass in the glass transition range is considered in the FE-Model. The structural relaxation is taken into account using the model of Narayanaswamy (1971). For the simulation of the tempering process the FE-Model of the glass plate was given an initial temperature of $T_0 = 650\,°\mathrm{C}$ and cooled down to the ambient temperature of $T_\infty = 25\,°\mathrm{C}$. The time increments Δt needed for converged results of the tempering process for different glass thicknesses were given in Pourmoghaddam and Schneider (2018). The resulting time–temperature relationship was put in terms of load steps on a structural mechanical model to calculate the stress response due to the tempering process. The different heat transfer coefficients were determined for yielding a residual surface compressive stress as shown in Fig. 7.

2.1.2 Engine power of the tempering oven

The glass plates were tempered in groups of three using the thermal tempering oven of the company Semcoglas Holding GmbH. In order to achieve different heat

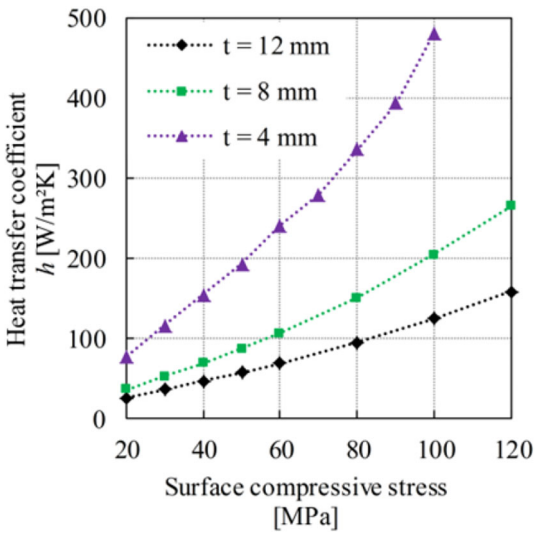

Fig. 7 Heat transfer coefficient [W/m^{2}K] versus surface compressive stress [MPa] from FE simulations

transfer coefficients for achieving the selected target residual stresses different cooling air velocities were calculated using the empirical equations suggested by Martin (1977). Once the cooling air velocity w for different target residual stress states is determined, the air pressure P can be calculated. After the determination of the required air pressure for each target residual stress considering the cooling air velocity and the heat transfer coefficient, the air pressure was matched to the experience curve of the thermal tempering oven in terms of the correlation between the engine power as the percentage of the total power of the thermal tempering oven and the resulting air pressure in the height of the air jets. The eight target residual mid-plane tensile stresses, which were plotted in Fig. 5 and the corresponding heat transfer coefficients, cooling air velocities and subsequently the required engine powers are summed up in Table 2 for the three thicknesses of 4, 8 and 12 mm. For the determination of the air pressure

Table 2 Target residual mid-plane tensile stresses σ_m [MPa] and the corresponding heat transfer coefficients h [W/m^{2}K], cooling air velocities w [m/s] and the required engine power P [%] as the percentage of the total power, atmospheric pressure and 25 °C ($\rho = 1.184$ kg/m^3)

No.	$t = 4$ mm				$t = 8$ mm				$t = 12$ mm			
	σ_m [MPa]	h [W/m^{2}K]	w [m/s]	P/total [%]	σ_m [MPa]	h [W/m^{2}K]	w [m/s]	P/total [%]	σ_m [MPa]	h [W/m^{2}K]	w [m/s]	P/total [%]
1	10	76.8	9.0	6.6	10	35.5	5.0	4.0	10	25.0	4.0	3.3
2	15	115.2	16.0	12.1	15	51.8	9.0	6.6	15	35.0	6.0	4.7
3	20	153.6	25.0	19.7	20	67.7	13.0	9.9	20	45.6	9.0	6.8
4	25	192.0	35.0	28.8	25	86.4	19.0	14.7	25	56.6	13.0	9.4
5	30	240.0	49.0	42.1	30	106.1	26.0	20.7	30	68.5	17.0	12.9
6	35	278.4	61.0	54.0	40	149.8	44.0	37.0	40	94.2	27.0	21.9
7	40	335.0	78.0	71.3	50	203.5	70.0	62.9	50	123.8	41.0	34.6
8	45	393.6	103.0	97.8	60	264.0	102.0	97.2	60	157.4	59.0	52.0

an atmospheric pressure and the temperature of 25 °C was assumed ($\rho = 1.184$ kg/m^3).

2.2 Stress measurements

In order to check the actual stress state in the specimens the residual stresses were measured after the tempering process using a scattered light polariscope (SCALP) developed by GlasStress Ltd. The residual stresses in vertical and horizontal direction in thirteen measurement points were measured at both surfaces of the specimens, see Fig. 8. The anisotropy of the residual compressive surface stresses in the area of the measurement points was quite low with a coefficient of variation around 3%. In Fig. 9, the optical path difference under polarized light is shown for three different thicknesses. It was observed that the anisotropy and the inaccuracies in yielding the target residual stresses increased for the 12 mm thick plates. In Fig. 10, the target residual stresses in comparison to the average of the measured mid-plane tensile stresses in the measurement points after the tempering process is shown.

Due to the lack of accuracy of the thermal tempering oven for the low engine power range, it was not possible to reach the lowest target residual stress states, especially for the 12 mm thick plates, see Fig. 10. However, considering the objective of yielding different residual stresses for a reasonable fragmentation analysis, the heat treatment of the specimen series was both necessary and successful.

3 Fracture tests

3.1 Fragmentation and fracture patterns

The heat treated series were fractured by impact according to EN 12150-1, see Fig. 11. The fracture tests were carried out using the *CulletScanner* of the Company SoftSolution GmbH, Fig. 12b. The glass plates were fixed at each edge on the *CulletScanner* desk and then fractured by impact. In order to keep the influence of the supplied energy uniform and low throughout all series, it was qualitatively ensured that the impact velocity of the grain remains constant for all samples. The *CulletScanner* desk is equipped with a scanner head, which can be driven over the fractured glass plate and scan the fracture pattern. Some examples of the scanned fracture

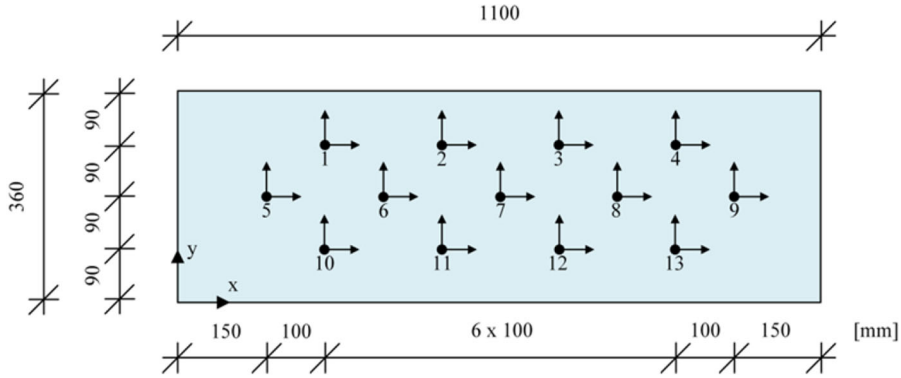

Fig. 8 Positions and directions of the residual stress measurements

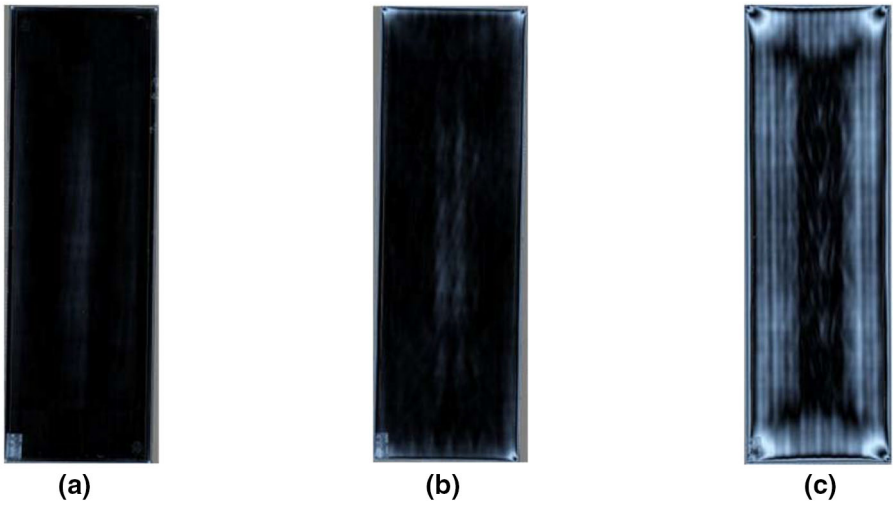

Fig. 9 Optical path difference under polarized light, **a** $t = 3.8$ mm, $\sigma_s = -91.3$ MPa (rel. deviation of 1.28%), **b** $t = 7.9$ mm, $\sigma_s = -91.1$ MPa (rel. deviation of 1.15%), **c** $t = 12.0$ mm, $\sigma_s = -97.4$ MPa (rel. deviation of 2.01%)

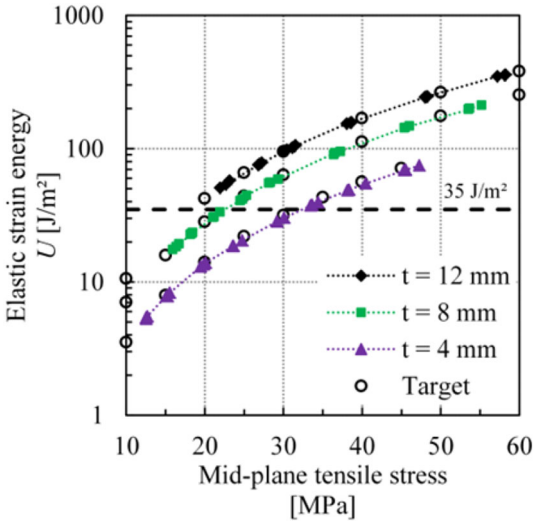

Fig. 10 Elastic strain energy U [J/m^2] versus mid-plane tensile stress [MPa], colored points show the average residual mid-plane stress from thirteen measurement points, hollow circles show the target residual mid-plane stress from Fig. 5, $U = 35$ J/m^2 is the start of the crack branching (Fineberg 2006)

patterns are shown in Figs. 13, 14 and 15. Subsequently, the fracture patterns were analyzed using the software CulletScanner (2017), which can, inter alia, count the fragments in selected observation fields.

The residual mid-plane tensile stresses in Figs. 13, 14 and 15 are the average values of the thirteen measurement points according to Fig. 8. The elastic strain energy U was calculated using the Eq. (3) for the average residual mid-plane tensile stresses and the corresponding thicknesses. For the same thickness the fracture structure becomes finer with the increase of the residual mid-plane stress, Fig. 13. The scans in Figs. 14 and 15 show that the same residual stress results in different fracture patterns respectively different fragment densities due to the different elastic strain energies for different glass thicknesses. Thus, the residual mid-plane stress of approx. 29 MPa creates a relatively fine fracture structure for a 12 mm thick glass plate, whereas for a 4 mm thick glass plate it just creates a few through cracks.

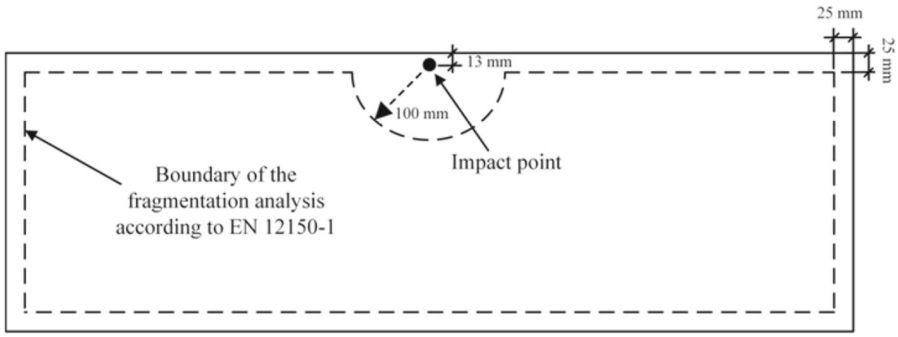

Fig. 11 The position of the Impact point according to EN 12150-1, the area, which is excluded from the fragmentation analysis according to EN 12150-1 is indicated by the dashed line

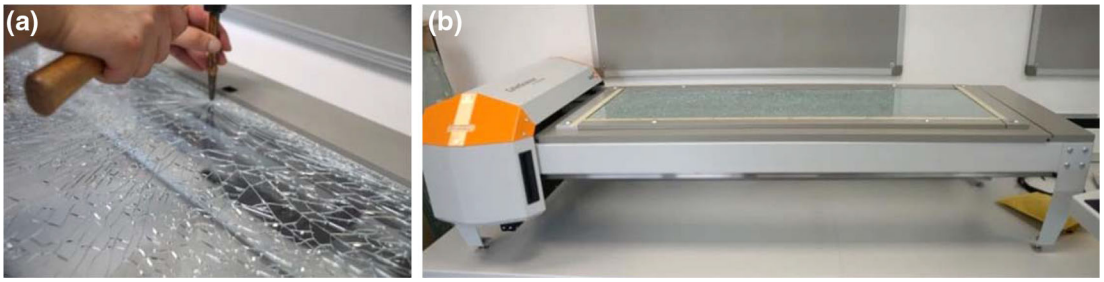

Fig. 12 **a** Fracture test, **b** *CulletScanner* desk of the company Soft Solution GmbH

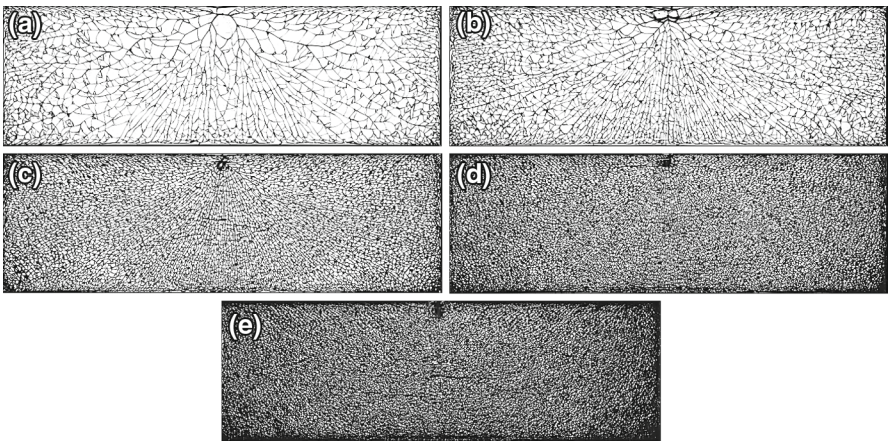

Fig. 13 Scans of the fracture patterns; plate thickness $t = 12$ mm; avg. measured residual mid-plane stresses σ_m (strain energy U [J/m^2]): **a** $\sigma_m = 26.9$ MPa; ($U = 76.4$ J/m^2). **b** $\sigma_m = 30.0$ MPa; ($U = 95.0$ J/m^2). **c** $\sigma_m = 38.1$ MPa; ($U = 153.3$ J/m^2). **d** $\sigma_m = 48.1$ MPa; ($U = 244.3$ J/m^2). **e** $\sigma_m = 58.3$ MPa; ($U = 358.9$ J/m^2)

3.2 Observation field

According to EN 12150-1 the fragments with in the dashed line, as shown in Fig. 11, should be taken into account for the evaluation of the fragment density. However, we observed that in the area below the impact point over the whole width to the opposite edge of the specimen, the branching and thus the fragment density is influenced by the low distance of the impact point and the opposite edge. The cracks propagate in direction of the opposite edge and have to branch more often along the width of the specimen than along its length to release energy. In specimens with a higher energy state and the same impact the crack propagation and branching from the location of the impact is much more intensive so that the described effect is less important

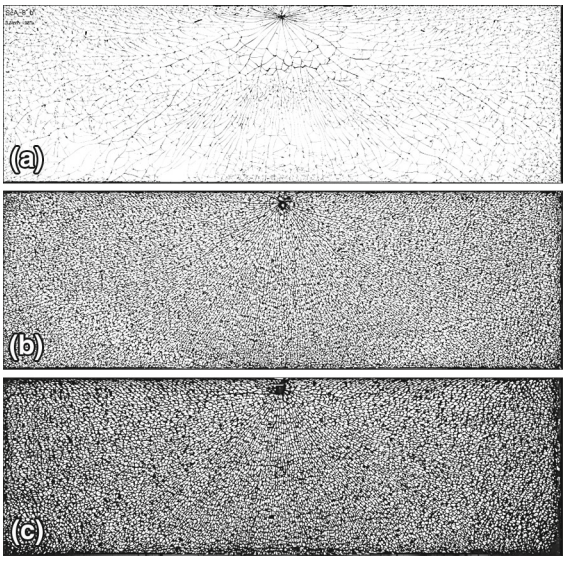

Fig. 14 Scans of the fracture patterns; different thicknesses; avg. measured residual mid-plane stress $\sigma_m \approx 45$ MPa (strain energy U [J/m^2]): **a** $\sigma_m = 45.3$ MPa; $t = 4$ mm; ($U = 72.2$ J/m^2). **b** $\sigma_m = 45.5$ MPa; $t = 8$ mm; ($U = 145.7$ J/m^2). **c** $\sigma_m = 48.1$ MPa; $t = 12$ mm; ($U = 244.3$ J/m^2)

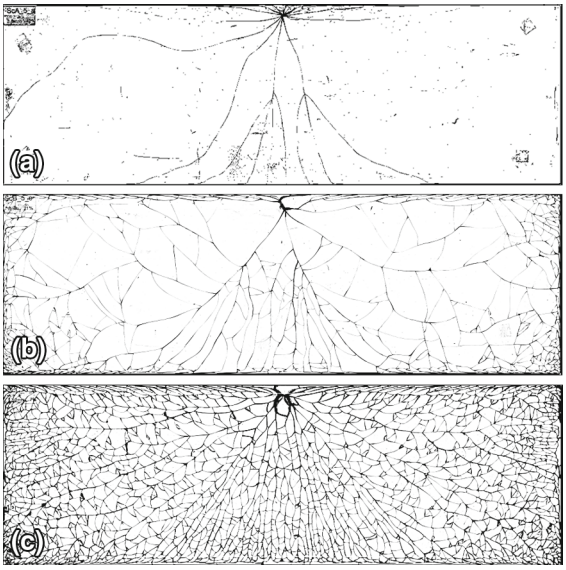

Fig. 15 Scans of the fracture patterns; different thicknesses; avg. measured residual mid-plane stress $\sigma_m \approx 29$ MPa (strain energy U [J/m^2]): **a** $\sigma_m = 29.2$ MPa; $t = 4$ mm; ($U = 30.0$ J/m^2). **b** $\sigma_m = 29.3$ MPa; $t = 8$ mm; ($U = 60.4$ J/m^2). **c** $\sigma_m = 27.2$ MPa; $t = 12$ mm; ($U = 78.1$ J/m^2)

in determination of the fragment density. In Fig. 16a, the area in which the fragmentation is influenced by the low distance of the impact point and the opposite edge of the specimen (impact influence zone) is shown for one fragmented specimen. Therefore, in this work only the fragments in the areas under an assumed angle of 45° left and right from the impact point were considered for the investigations. For the fragmentation analysis of the fractured tempered glass specimens the fragment density was determined for each specimen in eight observation fields with the size of 50 mm × 50 mm positioned around the measurement points 1, 4, 5, 6, 8, 9, 10 and 13 within the chosen boundary of the fragmentation analysis. The observation fields are shown in Fig. 16b. The reason for the eight observation areas was to have more fragments per specimen for quantitative results of the investigations.

Since our objective was to analyze fragmentation with just the influence of the residual stress state on the crack propagation and crack branching, the fragments in the chosen observation fields were assumed to be caused free from the impact energy as well as from the distance of the impact point and the edge of the specimen.

4 Experimental results

4.1 Fragment density

The fragment density was evaluated for the fractured specimens in terms of the average fragment number within the eight observation fields of each specimen. In Fig. 17a, the correlation between the evaluated average fragment density N_{50} in the observation fields with the size of 50 mm × 50 mm according to Fig. 16b and the mid-plane tensile residual stress of the specimens is presented. The solid curves show trend lines of the experimental data with the corresponding function and coefficient R^2. In Fig. 17b, the fragment density is shown in correlation with the elastic strain energy of the fragmented specimens according to Eq. (3). Also here the trend lines are added with the corresponding function and coefficient of determination R^2. The trend lines of the elastic strain energy values converge to approx. $U = 50$ J/m^2 for $N_{50} = 1$, which is recognized as the minimum required strain energy for fragmentation in an observation field. This value is plausibly greater than the energy of 35 J/m^2, which is needed for the start

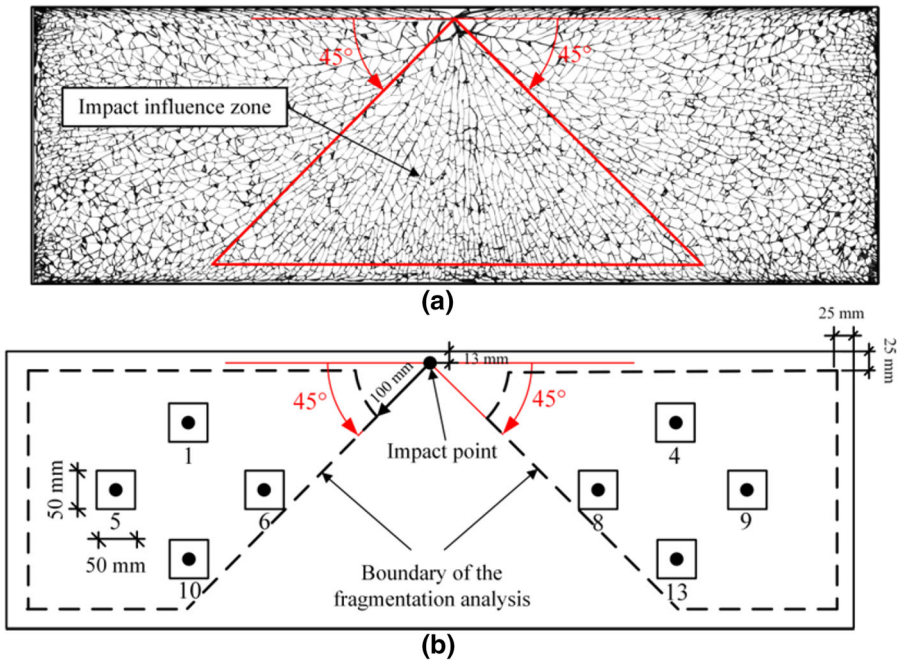

Fig. 16 **a** Impact influence zone under 45° left and right from the impact point. Fragmented specimen: $\sigma_m = 38.5$ MPa; $t = 12$ mm; ($U = 156.7$ J/m^2), **b** boundary of the fragmentation analysis. Eight observation fields with the size of 50 mm × 50 mm around the measurement points 1, 4, 5, 6, 8, 9, 10 and 13 under an angle of 45° from the impact point

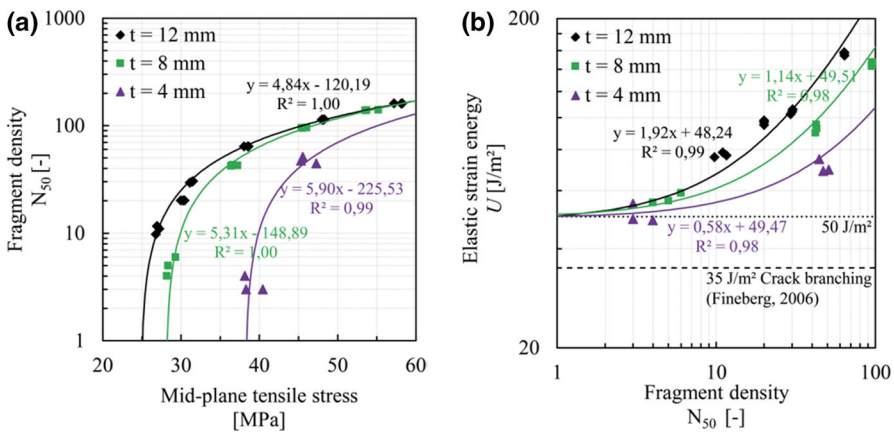

Fig. 17 **a** Fragment density N_{50} [-] versus mid-plane tensile stress [MPa]; the dots show the experimental data for the plate thicknesses $t = 4$ mm, $t = 8$ mm and $t = 12$ mm; solid curves are trend lines including the corresponding function and coefficient of determination R^2. **b** Elastic strain energy U [J/m^2] versus fragment density N_{50} [-]; solid curves are trend lines; the dashed line represents the start of crack branching according to Fineberg (2006) by 35 J/m^2; the trend lines converge to approx. 50 J/m^2 for $N_{50} = 1$.

of the local branching of a propagating crack determined by Fineberg (2006). The elastic strain energy boundary of fragmentation in an observation field and the corresponding required residual mid-plane tensile stresses for the plate thicknesses $t = 4$ mm (37.7 MPa), $t = 8$ mm (26.7 MPa) and $t = 12$ mm (21.8 MPa) are shown in Fig. 18.

The curves in Fig. 20 were determined due to the conversion of the Eq. (3) to:

$$\sigma_m = \sqrt{\frac{5}{4}\frac{E}{(1-\nu)}\frac{U}{t}} \tag{4}$$

As it was shown in Fig. 17b, the same elastic strain energy provides for a higher fragment density in thinner plates than in thicker plates. Or one can say that

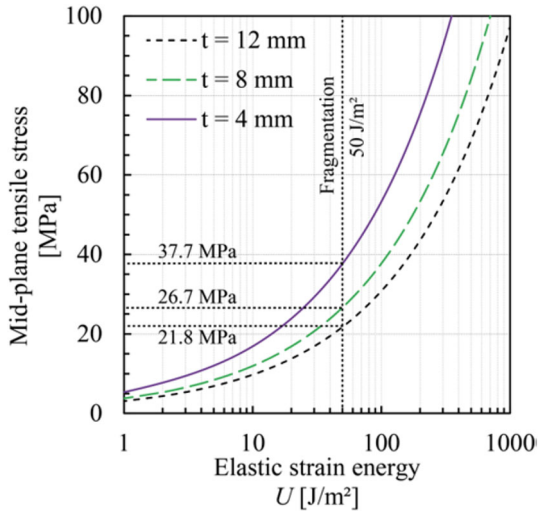

Fig. 18 Mid-plane tensile stress [MPa] versus elastic strain energy U [J/m^2]; the minimum fragmentation limit of approx. 50 J/m^2 in an observation field and corresponding mid-plane tensile stresses for the plate thicknesses $t = 4$ mm (37.7 MPa), $t = 8$ mm (26.7 MPa) and $t = 12$ mm (21.8MPa) are marked

in thinner plates a lower strain energy state provides for the same fragment density as in thicker plates. The reason is that the elastic strain energy is linearly proportional to the thickness but square proportional to the residual mid-plane tensile stress. In order to achieve the same elastic strain energy in thinner plates as in thicker plates, a corresponding higher residual mid-plane tensile stress in thinner plates is required, see Fig. 18.

According to EN 12150-1 for the classification of glass as thermally tempered single-pane safety soda-lime-silica glass the counted number of fragments in the observation field should not be less than 40 pcs for the plate thicknesses from 4 to 12 mm. However, the residual stress state and the corresponding elastic strain energy vary for different thicknesses. In Table 3, some fragment numbers N_{50} in correlation with the elastic strain energy U and the residual mid-plane tensile stress σ_m are listed.

4.2 Particle weight and particle shape

After the fragmentation fragments were collected for weighing. The average particle weight was determined from more than 130 particles per specimen chosen at random in the observation fields. The fragments were weighed using a precision scale with a weighing range of 0.02–220 g. The particle weight can be used in determining the degree of tempering. The correlation of mid-plane tensile stress and average particle weight in the thermally tempered glass plates is shown in Fig. 19. On the basis of the knowledge about the residual mid-plane tensile stress and the elastic strain energy release rate combined with the assumption that a fragment of fractured tempered glass has a hexagonal cross section with sides equal to the length of the average mean fracture path, Barsom (1968) suggests the mid-plane tensile stress σ_m to the power of four multiplied with the mass of a glass fragment M normalized with the thickness t to be constant:

$$\sigma_m^4 \times \left(\frac{M}{t}\right) = 7.73 \times 10^{12} \frac{lb^5}{in.^9} \tag{5}$$

The Eq. (5) converted to the fragment mass M can be rewritten as:

$$M = \left(\frac{t}{\sigma_m^4}\right) \times 7.73 \times 10^{12} \times Psi^4 \frac{lb}{in.} \tag{6}$$

with $Psi = \frac{lb}{in.^2} = 6.89 \times 10^{-3}$ MPa, $lb = 453.59$ g and $in. = 25.4$ mm the particle mass M can be written as:

$$M = \left(\frac{t}{\sigma_m^4}\right) \times 3.11 \times 10^5 \text{MPa}^4 \frac{\text{g}}{\text{mm}} \tag{7}$$

The particle weight, which was determined in this work, was compared to the predicted particle weight evaluated by means of the Eq. (7), see Fig. 19a. There-

Table 3 Fragment number N_{50} in correlation with the elastic strain energy U [J/m^2] and the residual mid-plane tensile stress σ_m [MPa]

N_{50} [-]	$t = 4$ mm		$t = 8$ mm		$t = 12$ mm	
	U [J/m^2]	σ_m [MPa]	U [J/m^2]	σ_m [MPa]	U [J/m^2]	σ_m [MPa]
20	61.2	41.7	72.1	32.0	86.4	28.6
40	72.6	45.4	95.3	36.8	125.0	34.4
80	95.9	52.2	140.7	44.7	201.7	43.7
120	119.2	58.2	186.0	51.4	279.0	51.4

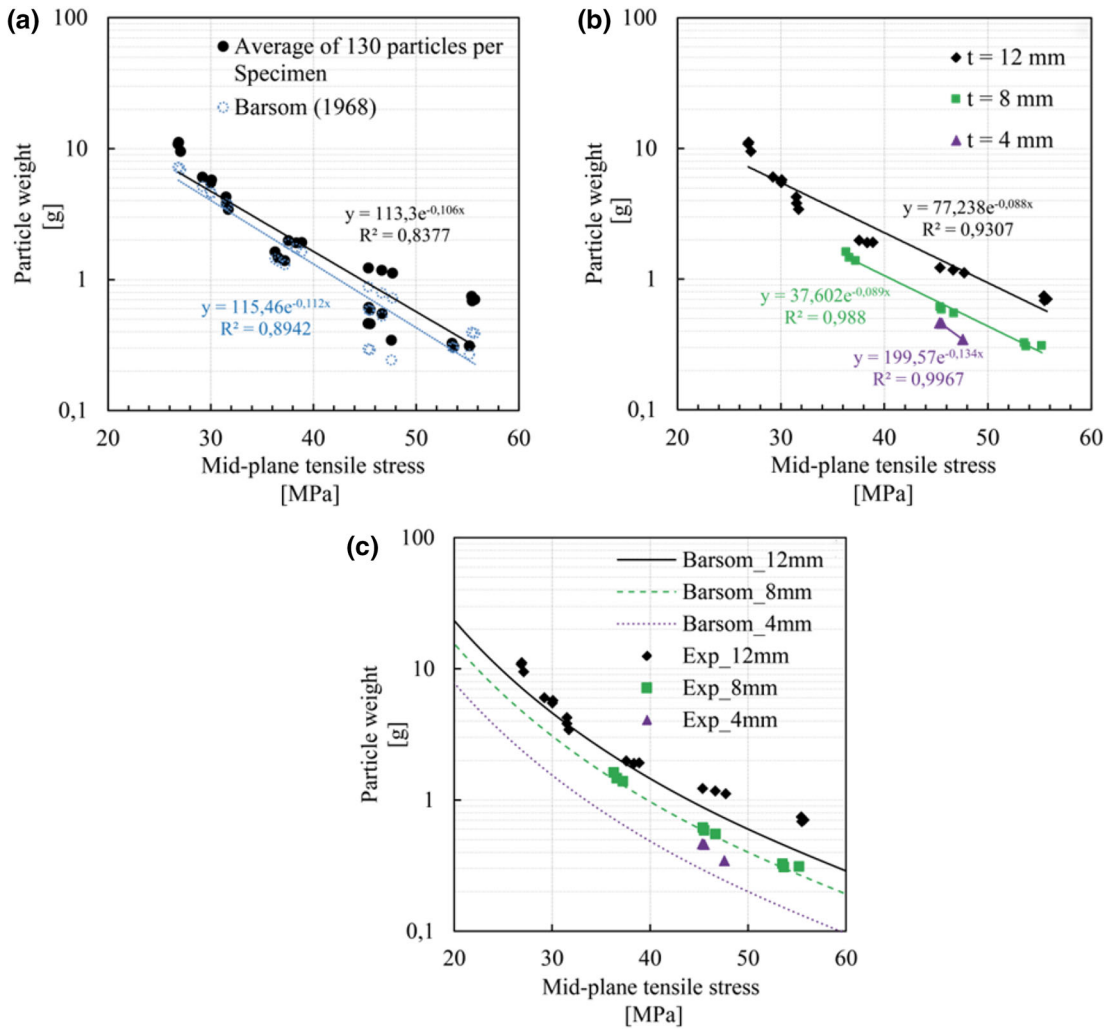

Fig. 19 Particle weight [g] versus mid-plane tensile stress [MPa]. **a** Experimental results of all fractured specimens in comparison with the particle weights evaluated by means of the Eq. (7) (Barsom 1968), **b** experimental results of the fractured specimens differentiated in thickness, **c** experimental results in comparison with the Eq. (7) evaluated for different thicknesses

fore, the residual mid-plane tensile stresses of the respective specimens were used for the evaluation. In Fig. 19b, the correlation between the particle weight and the residual mid-plane tensile stress is presented for each thickness differently. The Eq. (7) is evaluated for different thicknesses in Fig. 19c and compared with the experimental results. Knowing the density of glass (2500 kg/m^3) the volume of the fragments can be recalculated from the weight, Fig. 20a. Based on the influence of the residual stress state on the particle volume there is a corresponding influence of the residual state in a tempered glass on the size of the particles.

For a fragment with a cylindrical shape the radius r of the basic surface is determined and shown in Fig. 20b. The fragments created by the fracture have different basic surfaces with different numbers of edges n. Hence, a correlation between the particle base area for fragments with regular polygonal shapes $n = 3$ to $n = 8$ (Fig. 21) in addition to the cylindrical fragment ($n \rightarrow \infty$) is also determined and shown in Fig. 22.

The correlation was determined with the assumption that all fragments in the observation field have the same size or same number of edges n. Each curve in Fig. 22 represents a fragmented glass plate with the

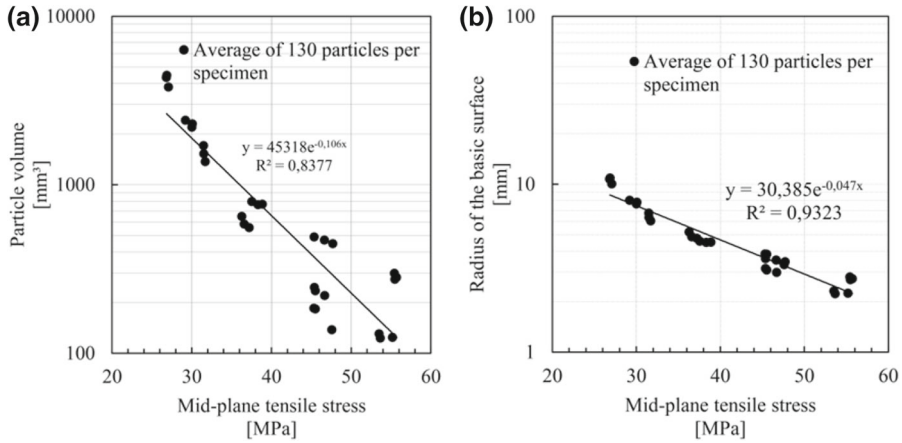

Fig. 20 **a** Particle volume [mm^3] versus mid-plane tensile stress [MPa] with volume $V = M/\rho$ and density $\rho = 2500\,\text{kg/m}^3$, **b** radius of the basic surface of a fragment with a cylindrical shape in [mm] versus mid-plane tensile stress [MPa]

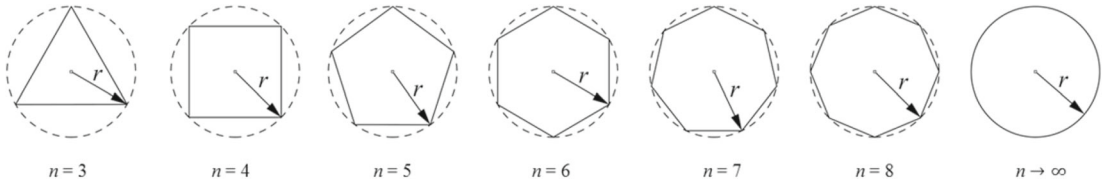

Fig. 21 Estimated particle shapes for the determination of the correlation between particle base surface and residual stress

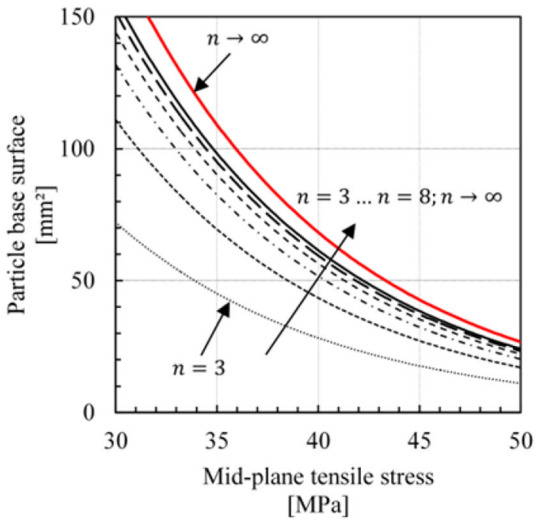

Fig. 22 Particle base surface [mm^2] versus mid-plane tensile stress [MPa] for fragment shapes with different numbers of edge $n = 3$ to $n = 8$ in addition to a cylindrical fragment ($n \to \infty$)

same edge number n. For the calculation of the particle base surface a surface radius r of a cylindrical fragment was recalculated from the particle volume. Using the radius r the base surface was calculated for different edge numbers n.

In reality the fragments in the observation field have different shapes with different edge numbers. However, with the assumption we want to show the influence of the residual stress on the base surface of the fragments.

5 Conclusion and future work

5.1 Summary and conclusion

This paper offered a comprehensive fragmentation analysis of thermally tempered soda-lime-silica glass. For the fragmentation analysis respectively the determination of the relation between the residual state in tempered glasses and the fragment density specimens were thermally tempered due to heat treatment of the specimens with different heat transfer coefficients. Residual stresses from low stress state to high stress state were selected as target stresses for three different thicknesses of $t = 4$ mm, $t = 8$ mm and $t = 12$ mm using the relationship between the residual stress and the elastic strain energy of the tempered glasses. In order to achieve different heat transfer coefficients respectively cooling rates for achieving the selected target residual stresses different cooling air velocities were calculated using the empirical equations suggested by Martin (1977). It was shown that these equations proved to be sufficiently accurate for the determination of the heat transfer coefficient in the case of

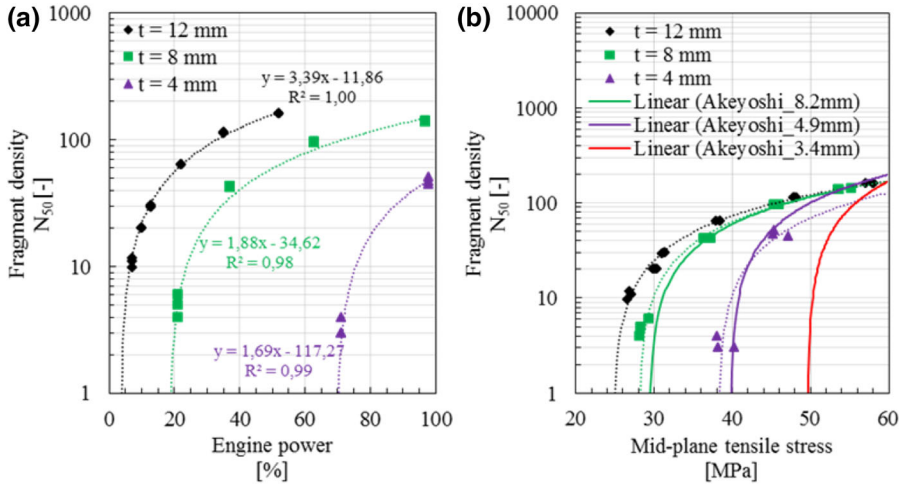

Fig. 23 **a** Fragment density N_{50} [-] versus engine power of the tempering oven [%]; the dots show the experimental data for the plate thicknesses $t = 4$ mm, $t = 8$ mm and $t = 12$ mm; dotted lines are trend lines including the corresponding function and coefficient of determination R^2. **b** Fragment density N_{50} [-] versus mid-plane tensile stress [MPa] in comparison with Akeyoshi and Kanai (1965) (solid lines)

impact flow. After the thermal tempering, the mid-plane tensile stress as well as the surface compressive stress was measured using the scattered light polariscope (SCALP). It was observed that the accuracy of the thermal tempering with respect to the deviation from the target residual stress decreases for thicker plates.

The heat treated specimens were fractured by impact and the fracture patterns were scanned using the *CulletScanner* of the company SoftSolution GmbH. The correlation of the residual stress with the fragment density was determined. For this purpose, the average number of fragments in eight selected observation fields of size 50 mm × 50 mm was determined for each specimen. In Fig. 23a, the relation between the fragment density and the setting engine power for the thermal tempering is shown. In Fig. 23b, the experimental results in this paper are compared with the experimental results from Akeyoshi and Kanai (1965).

Furthermore, independent of the plate thickness a minimum fragmentation limit of approx. 50 J/m^2, which was required for the fragmentation in the tempered glass specimens, was observed. Due to less crack branching and therefore very little to hardly existing fragmentation, tempered glass plates with an elastic strain energy lower than the stated value could not be considered for the fragmentation analysis.

Additionally, the influence of the residual stress state in tempered glass plates on the particle weight, particle volume and the particle size after the fragmentation was investigated. Assuming cylindrical fragments the radius of the fragments basic surface in correlation with the residual stress state was determined for the fractured specimens.

5.2 Future research

The results of the fracture tests shown in this paper will be used in further investigations to gain a better understanding of the fracture structure of thermally tempered glass. In the next step, a theoretical model based on the elastic strain energy conditions and the Voronoi tessellation to predict the macro-scale fragmentation in tempered glass will be validated with the experimental data compiled in this work. Further fracture tests are planned to analyze the fragmentation behavior and the impact influence on the fracture patterns at different impact loads and boundary conditions.

With regard to the fracture surface of the fragments, we intend to scan selected fragments collected here with the help of computer tomography (CT) and to examine and measure the actual fracture surface in detail. The aim is to establish a correlation between the actual fracture surface and the residual state. We also intend to carry out fractographic investigations on the fragments and establish correlations between the fractographic elements of the fracture surface and the residual stress state.

Compliance with ethical standards

Conflict of interest The authors declare that they have no conflict of interest.

References

Acloque, P.: Deferred processes in the fragmentation of tempered glass. In: Proceedings of the 4th International Glass Congress, vol. 6, pp. 79–291 (1956)

Akeyoshi, K., Kanai, E.: Mechanical properties of tempered glass. In: Proceedings of the 7th International Glass Congress, vol. 14, pp. 80–85 (1965)

Aronen, A.: Modelling of deformations and stresses in glass tempering. Ph.D. thesis, Julkaisu-Tampere University of Technology, Publication 1036 (2012)

Aronen, A., Karvinen, R.: Effect of glass temperature before cooling and cooling rate on residual stresses in tempering. Glass Struct. Eng. (2017). https://doi.org/10.1007/s40940-017-0053-6

Barsom, J.M.: Fracture of tempered glass. J. Am. Ceram. Soc. **51**(2), 75–78 (1968). https://doi.org/10.1111/j.1151-2916.1968.tb11840.x

CulletScanner: Version 17.4 (r40671) SoftSolution GmbH (2017)

EN 12150-1: Glass in building – Thermally toughened soda lime silicate safety glass – Part 1: definition and description; German version EN 12150-1 (2015)

Fineberg, J.: The dynamics of rapidly moving tensile cracks in brittle amorphous material. In: Shukla, A. (ed.) Dynamic Fracture Mechanics. World Scientific, Singapore, pp. 104–146 (2006)

Gulati, S.T.: Frangibility of tempered soda-lime glass sheet. Glass Performance Days, pp. 13–15 (1997)

Lee, H., Cho, S., Yoon, K., Lee, J.: Glass thickness and fragmentation behavior in stressed glasses. New J. Glass Ceram. **2**, 138–143 (2012)

Martin, H.: Heat and mass transfer between impinging gas jets and solid surfaces. Adv. Heat Transf. **13**, 1–60 (1977). https://doi.org/10.1016/S0065-2717(08)70221-1

Mognato, E., Brocca, S., Barbieri, A.: Thermally processed glass: correlation between surface compression, mechanical and fragmentation test. Glass Performance Days, pp. 8–11 (2017)

Narayanaswamy, O.S.: A model of structural relaxation in glass. J. Am. Ceram. Soc. **54**(10), 491–498 (1971). https://doi.org/10.1111/j.1151-2916.1971.tb12186.x

Nielsen, J.H., Olesen, J.F., Stang, H.: The fracture process of tempered soda-lime-silica glass. Exp. Mech. **49**(6), 855–870 (2009a). https://doi.org/10.1007/s11340-008-9200-y

Nielsen, J.H.: Tempered glass: bolted connections and related problems. Ph.D. thesis, Technical University of Denmark, Department of Civil Engineeing (2009b)

Nielsen, J.H.: Remaining stress-state and strain-energy in tempered glass fragments. Glass Struct. Eng. **2**, 45–56 (2017). https://doi.org/10.1007/s40940-016-0036-z

Nielsen, J.H., Olesen, J.F., Poulsen, P.N., Stang, H.: Finite element implementation of a glass tempering model in three dimensions. Comput. Struct. **88**(17–18), 963–972 (2010). https://doi.org/10.1016/j.compstruc.2010.05.004

Pourmoghaddam, N., Nielsen, J.H., Schneider, J.: Numerical simulation of residual stresses at holes near edges and corners in tempered glass? A parametric study. In: Engineered Transparency International Conference at Glasstec, pp. 513–525 (2016)

Pourmoghaddam, N., Schneider, J.: Finite-element analysis of the residual stresses in tempered glass plates with holes or cut-outs. Glass Struct. Eng. [Online]. https://doi.org/10.1007/s40940-018-0055-z (2018)

Schneider, J.: Festigkeit und Bemessung punktgelagerter Gläser und stoßbeanspruchter Gläser. Ph.D. thesis, Technische Universität Darmstadt (2001)

Shutov, A.I., Popov, P.B., Bubeev, A.B.: Prediction of the character of tempered glass fracture. Glass Ceram. **55**(1–2), 8–10 (1998). https://doi.org/10.1007/BF03180135

Tandon, R., Glass, S.J.: Fracture Mechanics of Ceramics; Active Materials, Nanoscale Materials, Composites, Glass, and Fundamentals, vol. 14, pp. 77–92. Springer, Berlin (2005)

Warren, P.D.: Fragmentation of Thermally Strengthened Glass. Fractography of Glasses and Ceramics IV, pp. 389–402. The American Ceramic Society, Westerville (2001)

Publisher's Note Springer Nature remains neutral with regard to jurisdictional claims in published maps and institutional affiliations.